Research Square

Preprints are preliminary reports that have not undergone peer review.
They should not be considered conclusive, used to inform clinical practice,
or referenced by the media as validated information.

Identification and validation of key genes of Xiaozhengtongluo formula in the treatment of diabetic nephropathy by Mendelian randomization

Zhao Liu
Hebei Provincial Hospital of Traditional Chinese Medicine
Moxixuan Liu
Hebei University of Chinese Medicine
Haina Wu
Hebei Provincial Hospital of Traditional Chinese Medicine
Ying Zhang
Hebei Provincial Hospital of Traditional Chinese Medicine
Zhiqiang Chen
chenzhqiang2011@163.com
Hebei Provincial Hospital of Traditional Chinese Medicine
Xiaona Wei
Hebei Provincial Hospital of Traditional Chinese Medicine
Yun Ma
Hebei Provincial Hospital of Traditional Chinese Medicine
Xinai Wang
Hebei Provincial Hospital of Traditional Chinese Medicine
Hui Gao
Hebei Provincial Hospital of Traditional Chinese Medicine
Jinmei Zheng
Hebei Provincial Hospital of Traditional Chinese Medicine
Jing Liang
Hebei Provincial Hospital of Traditional Chinese Medicine

Research Article

Keywords: Diabetic nephropathy, Xiaozhengtongluo formula, Network pharmacology, Mendelian randomization, Regulatory network

Posted Date: July 7th, 2026

DOI: https://doi.org/10.21203/rs.3.rs-10003284/v1

License: This work is licensed under a Creative Commons Attribution 4.0 International License.
Read Full License

Additional Declarations:
No competing interests reported.

Tables 1 to 5 are available in the supplementary files section

Identification and validation of key genes of Xiaozhengtongluo formula in the treatment of diabetic nephropathy by Mendelian randomization

Zhao Liu[1,2], Moxixuan Liu[2], HainaWu[1], Ying Zhang[1], Zhiqiang Chen*[1,2],

Xiaona Wei[1], Yun Ma[1], Xinai Wang[1], Hui Gao[1], Jinmei Zheng[1], Jing Liang[1]

(Zhao Liu and Moxixuan Liu should be considered joint first authors)

Affiliations

1 Hebei Provincial Hospital of Traditional Chinese Medicine, Shijiazhuang, P. R. China

2 Hebei University of Chinese Medicine, Shijiazhuang, P. R. China

E-mail Address

Zhao Liu, E-mail: yjs20223023@hebcm.edu.cn

Moxixuan Liu, E-mail: liumoxixuan@hebcm.edu.cn（Co-first author）

Zhiqiang Chen*, E-mail: chenzhqiang2011@163.com（Corresponding Author）

Clinical trial number: not applicable

Abstract

Background: Xiaozhengtongluo formula (XZTL) has a positive effect on the treatment of diabetic nephropathy (DN), but its mechanism is not fully understood. Therefore, it is important to explore the key genes of XZTL in the treatment of DN.

Methods: Differentially expressed genes (DEGs) between DN and control obtained from GSE96804, drug target genes of XZTL, and disease target genes of DN obtained from public databases were intersected. Genes of intersection were defined as candidate genes. Next, Mendelian randomization (MR) analysis was used to ascertain the causal associations between candidate genes and DN. Afterwards, key genes were confirmed through receiver operating characteristic (ROC) curve analysis and expression validation. Subsequently, enrichment analysis, molecular regulatory network analysis, and molecular docking were conducted. Finally, experimental verification of the expression levels of key genes was performed through reverse transcription-quantitative polymerase chain reaction (RT-qPCR).

Results: Altogether, 29 candidate genes were described and subjected to the MR analysis, and three key genes (APOD, IGFBP3, LPL) were identified. IGFBP3 was risk factor for DN. LPL and APOD were the protective factors of DN. All three key genes were co-enriched in 26 pathways, such as oxidative phosphorylation and heme metabolism. Regulatory networks for key genes included that MIR497HG regulated IGFBP3 by regulating hsa-miR-19a-3p and NEAT1 regulated LPL by regulating

hsa-miR-29a-3p. IGFBP3 and LPL were co-regulated by two transcription factors, including SP3 and SP1. Then, Molecular docking results showed that APOD bound to baicalein, LPL bound to oleic acid, and IGFBP3 bound to quercetin. This suggested that baicalein, oleic acid, and quercetin in XZTL had the potential for DN therapy. Following, RT-qPCR results demonstrated aberrant expression of IGFBP3, APOD, and LPL in the DN state, and the expression of these three genes was restored to normal levels in the XZTL intervention group.

Conclusion: In this study, three key genes (APOD, IGFBP3, and LPL) of XZTL in the treatment of DN were finally obtained, which provided a reference for the mechanism of XZTL in the treatment of DN.

Keywords: Diabetic nephropathy, Xiaozhengtongluo formula, Network pharmacology, Mendelian randomization, Regulatory network

1. Introduction

Diabetic nephropathy (DN), one of the most predominant microvascular complications of diabetes mellitus (DM), has an incidence of approximately 20% to 40%(B. Li et al., 2023). With the global surge in the prevalence of DM, DN has become the leading cause of hospitalization among patients with chronic kidney disease (CKD), posing a severe threat to public health(X.-X. Zhang et al., 2020). DN progresses insidiously from glomerular hyperfiltration to microalbuminuria, proteinuria and progressive renal dysfunction(Reutens & Atkins, 2011).

Although drugs recommended by the American Diabetes Association (ADA) guidelines, including angiotensin-converting enzyme inhibitors (ACEIs), angiotensin II receptor blockers (ARBs), sodium-glucose cotransporter 2 inhibitors (SGLT2is), and novel non-steroidal selective mineralocorticoid receptor antagonists (MRAs), have been successively applied in clinical practice, they still fail to effectively halt the progression of DN(Kim et al., 2022). The pathogenesis of DN is associated with the synergistic regulation of multiple pathways, such as oxidative stress, podocyte injury, and renin-angiotensin-aldosterone system (RAAS) dysregulation, yet the key molecular nodes remain not fully elucidated(Dwivedi & Sikarwar, 2025). In recent years, with the continuous improvement of clinical research on traditional Chinese medicine (TCM), the role of TCM in the prevention and treatment of DN has gradually become a research hotspot(X.-J. Liu et al., 2022). According to TCM theory, the major pathological products of DN are the intermingling of phlegm and blood stasis. The Xiaozheng Tongluo formula (XZTL) is developed based on this theory, composed mainly of *Astragali Radix, Atractylodis Macrocephalae Rhizoma, Angelicae Sinensis Radix, Chuanxiong Rhizoma, Salviae Miltiorrhizae Radix et Rhizoma, Carthami Flos and Fritillariae Thunbergii Bulbus*. Modern pharmacological studies demonstrate that active components of these medicinal herbs target the core pathogenesis of diabetic nephropathy. Astragalus membranaceus and astragaloside attenuate renal oxidative stress via Nrf2, inhibit fibrosis through TGF-β1/Smad2/3, reduce proteinuria, and improve renal function(X. Zhang et al., 2024) . Salvia miltiorrhiza extract suppresses inflammation and fibrosis by activating PPAR-α/PPAR-γ and downregulating TGF-β1 and IL-1β (Hsu et al., 2024) . Ligustilide from Chuanxiong relieves oxidative stress via Nrf2 and inhibits

inflammation and apoptosis through p38/ERK MAPK (Qi et al., 2024). Angelica polysaccharides mitigate mesangial proliferation and inflammation by inhibiting NF-κB and RAGE and upregulating BMP-7 to preserve renal function(Sui et al., 2019). These findings indicate that ingredients of XZTL act synergistically against diabetic nephropathy through antioxidant, anti-inflammatory, and antifibrotic pathways. Although XZTL shows significant clinical efficacy, its precise molecular targets and mechanisms remain poorly defined. Therefore, identifying key genes responsible for XZTL-mediated renal protection is critically important.

Network pharmacology (NP) is a discipline based on systems biology theory, integrating multi-omics and bioinformatics(Zhao et al., 2023). It constructs a *drug-component-target-disease* interaction network from a holistic perspective to screen core targets and elucidate regulatory mechanisms, thereby providing support for the design of multi-target drugs. Mendelian randomization (MR) is a causal inference method that uses genetic variants (single nucleotide polymorphisms, SNPs) as instrumental variables, whose reliability relies on three fundamental assumptions: relevance (SNPs are strongly associated with exposures), independence (SNPs are independent of confounding factors) and exclusion restriction (SNPs affect outcomes only through exposures)(Ference et al., 2021). This method can effectively circumvent confounding factors and reverse causality bias. Both approaches have been widely applied in DN and related diseases: the pathogenesis of DN involves multiple pathways including inflammation, oxidative stress and renal fibrosis, which is highly consistent with the NP concept of *multi-target and holistic regulation*. NP is often used to screen active components of TCM herbs (e.g., astragaloside IV, salvianolic acid B) and compound formula targets for DN treatment, as well as to predict core regulatory pathways(Sun et al., 2022). MR is mostly employed to verify the causal associations between candidate genes/metabolic indicators and DN, resolve controversies in previous studies and fill the gaps in causal inference(W. Zhang et al., 2024). Together, these two approaches provide important theoretical and experimental evidence for drug development and etiological investigation of DN.

Based on transcriptomic data from public databases, this study first screened differentially expressed genes between DN and control samples via differential expression analysis. Next, drug target-related genes were obtained from the chemical components of XZTL, and DN-associated target genes were retrieved from public databases. The intersection of the three gene sets yielded candidate targets of XZTL for DN treatment. MR analysis was then performed to further screen these candidate targets to identify key genes. A series of bioinformatics analyses were subsequently conducted to explore the key genes and potential regulatory mechanisms underlying the therapeutic effects of XZTL on DN, aiming to provide novel references for the clinical treatment of DN.

2. Materials and methods

2.1 Data collection

GSE96804 and GSE30528 datasets were retrieved in Gene Expression Omnibus (GEO) (https://www.ncbi.nlm.nih.gov) database. The GSE96804 dataset was derived from the GPL17586 platform and included 41 diabetic nephropathy (DN) and 20 control glomerular tissue samples. The GSE30528 dataset was derived from the GPL571 platform, including nine DN and 13 control glomerular tissue samples.

The ebi-a-GCST90018612 (DN) was obtained from the Integrative Epidemiology Unit Open genome-wide association study (IEU OpenGWAS) database (https://gwas.mrcieu.ac.uk/), including 132,984 samples of East Asian (220 DN samples and 132,764 control samples) and 12,447,074 single-nucleotide polymorphisms (SNPs).

2.2 Component of Xiaozhengtongluo formula (XZTL)

XZTL was the drug used in the present study, including *Astragalus membranaceus* (Fisch.) Bge., *Salvia miltiorrhiza* Bge, *Atractylodes macrocephala* Koidz., *Angelica sinensis* (Oliv.) Diels, *Ligusticum chuanxiong* Hort., *Carthamus tinctorius* L., and *Fritillaria thunbergii* Miq.

2.3 Identification and functional analyses of differentially expressed genes (DEGs)

The "limma" (v 3.58.1) (Ritchie et al., 2015) package was applied to acquire differentially expressed genes (DEGs) in the comparison between DN and control samples within GSE96804. The threshold values were $p < 0.05$ and $|\log2 \text{ fold change (FC)}| > 0.5$. A volcano plot was utilized to visually represent the DEGs through "ggplot2" (v 3.5.1) (Zheng & Huang, 2024) package, and the top 10 up- and down-regulated genes in the DN group, sorted according to Log2(FC), were labeled in the volcano plot. Additionally, the "ComplexHeatmap" (v 2.10.8) (Gu et al., 2016)package was used to draw the expression heat map of these 20 DEGs. Following, Gene Ontology (GO) and Kyoto Encyclopedia of Genes and Genomes (KEGG) enrichment analyses of DEGs were undertaken ($p < 0.05$) utilizing "clusterProfiler" (v 4.10.1)(Wu et al., 2021)package.

2.4 Acquisition of drug target genes and disease target genes

The active ingredients of XZTL were retrieved from the Traditional Chinese Medicine Systems Pharmacology (TCMSP) database (https://tcmsp.91medicine.cn/#/home). Ingredients with an Oral Bioavailability (OB) of 20% or higher and a Drug-Likeness (DL) score of 0.1 or above were selected as the efficacious active components of XZTL, and the "related targets" module of TCMSP was utilized to search potential targets of efficacious active ingredients. Then, the UniProt database (https://www.uniprot.org/uniprot/) was applied to obtain the gene names of these potential targets, which served as drug target genes.

To obtain target genes associated with DN, we searched for disease target genes in GeneCards (https://www.genecards.org/) and Therapeutic Target Database (http://db.idrblab.net/ttd/) using the keyword "diabetic nephropathy". The genes obtained from the retrieval of the two databases were summarized, and the duplicate genes were removed. These genes were recorded as disease target genes of DN.

2.5 Identification and functional analyses of candidate genes

The overlapping of DEGs, drug target genes, and disease target genes was achieved through the "ggvenn" (v 0.1.10)(Zheng et al., 2022) package. These overlapping genes were recorded as candidate genes, and a network was constructed according to the correlation among disease, candidate genes, efficacious active ingredients, and drugs. Subsequently, GO and KEGG enrichment analyses of candidate genes were also undertaken ($p < 0.05$) utilizing the "clusterProfiler" (v 4.10.1) package. Then, in order to explore the relationship among efficacious active components, candidate genes, and enriched pathways, the interaction network was constructed by combining efficacious active components, candidate genes, and the top five enrichment pathways ranked by count for each category

of GO. The network was displayed by Cytoscape (v 3.9.1)(Shannon et al., 2003).

2.6 Data preparation for Mendelian randomization (MR)

Expression quantitative trait loci (eQTL) data for candidate genes (exposure factors) were obtained from the IEU OpenGWAS database. The exposure factors were read by the extract_instruments function in “TwoSampleMR” (v 0.6.4) (Hemani et al., 2018) package, and SNPs significantly linked to the exposure factors were identified under the condition of p-value less than 5×10-6. SNPs with linkage disequilibrium (LD) were further eliminated using r2 < 0.001, kb > 10 kb, clump = TRUE. Exposure factors with SNP>3 and F>10 were also removed. Afterward, we excluded SNPs that were significantly associated with the outcome, as identified through GWAS data. The final obtained SNPs were used as IVs for MR analysis. The occurrence of DN was defined as the outcome.

2.7 MR analysis

The effect alleles and their corresponding sizes were standardized using the harmonise_data function within the “TwoSampleMR” (v 0.6.4) package. Then, MR analysis was carried out combining five algorithms [MR Egger (Xian et al., 2023), Weighted median (Z. Liu et al., 2023), Inverse variance weighted (IVW) (Mounier & Kutalik, 2023) , Weighted mode (Xu et al., 2022), Simple mode (Dai et al., 2023)] via the MR function to ascertain the relationship between exposure factors and outcome that indicated causation. The results of the IVW algorithm were mainly considered. The observed p-value and odds ratio (OR) value for IVW were noted, and $p < 0.05$ suggested a statistically significant causal link between candidate genes and DN. Forest plots, scatter plots, and funnel plots were used to further illustrate the MR consequence. Subsequently, to assess the credibility of MR findings, sensitivity analyses including heterogeneity test(N. Li et al., 2023) , horizontal pleiotropy assessment (Gan et al., 2023), and leave-one-out analysis (LOO)(Dong et al., 2023) were performed. In the MR heterogeneity test, the IVW Cochran's Q test yielded a p-value exceeding 0.05, indicating an absence of heterogeneity among candidate genes and DN. In the horizontal pleiotropy test, a p-value exceeding 0.05 suggested that the SNP did not have horizontal pleiotropy. The results were reliable if the overall effect of the LOO analysis did not appear to be significantly biased. Finally, to verify that the results of forward analysis were not confounded by reverse causality effects, the Steiger test was performed using the criteria for causality determination (TRUE and $p < 0.05$). The candidate genes that passed the Steiger test were selected as candidate key genes and kept for further analysis.

2.8 Expression verification and receiver operating characteristic (ROC) curve construction

In GSE96804 and GSE30528, to further evaluate the predictive performance of candidate key genes, the candidate key genes were selected to draw the ROC curve, which was performed using the "pROC" (v 1.18.5) (Robin et al., 2011) package. Meanwhile, the area under the curve (AUC) was determined. Genes with AUC > 0.7 and not equal to one in both datasets were delivered to the Wilcoxon test to analyze the expression levels between DN samples and controls in two datasets. Finally, genes with a consistent expression trend and significant differential expression ($p < 0.05$) in the two datasets were further defined as key genes.

2.9 Gene set enrichment analysis (GSEA)

We selected "h.all.V2023.2.Hs.Symbols.gmt" as the reference gene set and used "psych" (v 2.4.3) (Zein

& Akhtar, 2025) package to calculate the Spearman correlation coefficient of each key gene and all other genes in GSE96804. Then, all genes were sorted in descending order based on the correlation coefficients to obtain a list of correlated genes for each key gene. GSEA was performed using the "clusterProfiler" package (v 4.10.1) to explore the potential functions of key genes. |Normalized enrichment scores (NES)| > 1, false discovery rates (FDR) < 0.05 and p < 0.05 were the thresholds for significant enrichment. In order of p value, the top 10 enrichment pathways were selected for display using "enrichplot" (v 1.20.3) (J. Liu et al., 2024) package.

2.10 Chromosomal localization and functional similarity analysis

To explore the chromosomal localization of key genes, the "RCircos" (v 1.2.2) (H. Zhang et al., 2013) package was used for annotation and mapping, showing the distribution of key genes on chromosomes. Then, to identify the genes with similar functions to the key genes, the key genes were imported into the GeneMANIA (https://genemania.org/) database, and those genes that exhibited similar functionalities were identified.

2.11 Construction of molecular regulatory networks

To acquire a deeper insight into the molecular regulatory mechanisms underlying key genes, the microRNA (miRNA) interacting with the key genes (mRNA) was predicted by DIANA-microT (http://diana.imis.athena-innovation.gr/DianaTools/index.php) and miRDB (https://mirdb.org/) database. The predicted miRNAs in the two databases were intercrossed using the "ggvenn" (v 0.1.10) package. Next, the starBase (https://rnasysu.com/encori/) and miRNet (https://www.mirnet.ca/) databases were utilized for predicting the long non-coding RNAs (lncRNAs) that interact with miRNA. In combination with the above prediction, Cytoscape (v 3.9.1) was used to establish the molecular regulatory network consisting of lncRNA, miRNA, and mRNA. At the same time, we identified the potential transcription factors (TFs) associated with the key genes through the miRNet database, and Cytoscape (v 3.9.1) was used to visualize the key gene-TF regulatory network.

2.12 Molecular docking

In order to verify the degree of binding between the key genes and the efficacious active ingredients of the XZTL, molecular docking was performed. Firstly, the efficacious active ingredients corresponding to each key gene were sorted (based on OB value), and the top one of the corresponding component of each key gene was selected for molecular docking. Then, in the Protein Data Bank (PDB) (http://www.rcsb.org) and National Center for Biotechnology Information (NCBI) (https://www.ncbi.nlm.nih.gov/pccompound/) database, protein structure data of key genes and structure data of efficacious active ingredients were downloaded. Finally, the CB-Dock2 website (https://cadd.labshare.cn/cb-dock2/php/blinddock.php) was utilized for molecular docking of the key genes and efficacious active ingredients in the network mentioned above.

2.13 Reverse transcription-quantitative polymerase chain reaction (RT-qPCR)

To verify whether the differential expression of key targets in animal tissues following TCM intervention for DN was consistent with the bioinformatics results, Sprague-Dawley (SD) rats were used to establish a DN model via a high-fat diet combined with intraperitoneal injection of streptozotocin (STZ). Renal glomerular tissue samples were collected from 5 rats in each group: the

normal group (control group), DN group (disease group), and TCM-intervened DN group (Xiaozheng Tongluo group). The study was approved by the XXX (Ethical Approval No.: XXX). Quantitative real-time polymerase chain reaction (qRT-PCR) was performed to validate the expression levels of key targets, and the $2^{-}\Delta\Delta Ct$ method was used to calculate the differences in the expression levels of key targets among the control, disease, and intervention groups.

2.14 Statistical analysis

All analyses were executed utilizing the R programming language (v 4.3.1). The Wilcoxon test was applied to compare differences between the two groups, with a statistical significance threshold of $p < 0.05$.

3. Results

3.1 DEGs were enriched in 1715 GO pathways and 79 KEGG pathways

A total of 2,693 DEGs between DN and control were obtained, including 1,290 up-regulated genes, such as FN1, and 1,403 down-regulated genes, such as HBA1, in the DN group (Figure 1A-B). To further understand the potential biological roles and pathways of DEGs, altogether 1386 biological processes (BPs), 105 cell components (CCs), 224 molecular functions (MFs), and 79 KEGG pathways ($p < 0.05$) were identified. DEGs were mainly significantly enriched in small molecule catabolic process (BP), apical part of cell (CC), sulfur compound binding (MF), and fatty acid degradation (KEGG). Only the top five functions ranked by count value were shown in each part of the GO analysis. The top five pathways with the lowest p value in KEGG enrichment analysis were labeled **(Figure 1C-D)**. The full enrichment pathway information was shown in **Supplementary Table 1-2**.

3.2 The 29 candidate genes were enriched in 1256 GO pathways and 51 KEGG pathways

After prediction, 4,388 disease target genes and 488 drug target genes were obtained **(Supplementary Table 3-4)**. Altogether 29 intersection genes of 2,693 DEGs, 4,388 disease target genes, and 488 drug target genes were defined as candidate genes for subsequent analysis**(Figure 2A)**. Following, to understand the molecular functions and pathways of the candidate genes, enrichment analysis was conducted on 29 candidate genes. Altogether 1,129 BPs, 41 CCs, 86 MFs, and 51 KEGG pathways ($p < 0.05$) were identified. Candidate genes were mainly significantly enriched in response to oxidative stress (BP), membrane raft (CC), antioxidant activity (MF), and fluid shear stress and atherosclerosis (KEGG) **(Figure 2B-C)**. The full enrichment pathway information was shown in **supplementary Table 5-6**. Networks of diseases, candidate genes, effective active ingredients, and drugs were constructed. The network showed that 7 drugs obtained 150 effective active ingredients, such as MOL002694, and targeted 29 candidate genes, such as IGFBP3, for DN. PTGS1 was the gene targeted by the most effective active ingredients **(Figure 2D).** The network with efficacious active components, candidate genes, and enriched pathways contained 15 pathways, such as growth factor binding, in

addition to candidate genes and effective active ingredients **(Figure 2E).**

3.3 Screening of candidate key genes by MR

To obtain the candidate key genes, MR was performed on the candidate genes. Through the screening of SNPs, the eQTL data of 18 candidate genes were finally screened for subsequent analysis. Results based on the IVW algorithm, IGFBP3, APOD, CAV1, and LPL were significantly associated with DN ($p < 0.05$) **(Table 1).** In the scatter plot, APOD and IGFBP3 showed a positive slope, indicating that they were risk factors. CAV1 and LPL showed a negative slope, suggesting that they acted as protective factors. In the forest plot, the overall effect of IVW for CAV1 and LPL was less than 0, indicating that they were protective factors. The overall effect of IVW for APOD and IGFBP3 was more than 0, indicating that they were risk factors. The findings of the forest plot aligned with those of the scatter plot **(Figure 3A-B)**. In the funnel plots, the SNPs of the APOD, IGFBP3, and LPL were basically distributed symmetrically, which was in accordance with the second law of Mendelian randomization. CAV1 had a poor distribution status and was eliminated at this step **(Figure 3C)**. To evaluate the strength and reliability of the MR findings, a sensitivity analysis was performed. The results of the heterogeneity test indicated that there was no heterogeneity in LPL, IGFBP3, and APOD ($p > 0.05$) **(Table 2)**. The results of the horizontal pleiotropy test showed that there was no horizontal pleiotropy in LPL, IGFBP3, and APOD ($p > 0.05$) **(Table 3)**. The LOO analysis showed that the gradual elimination of each SNP resulted in little change in the effect of the remaining SNPs on the outcome variables, indicating that the results of the MR analysis for LPL, IGFBP3, and APOD were reliable and stable **(Figure 3D)**, and these three genes passed the sensitivity analysis. Then, to verify that the analysis results were not affected by reverse causality effects, we performed the Steiger test. The Steiger test for these three genes was TRUE ($p < 0.05$) **(Table 4)**. Therefore, LPL, IGFBP3, and APOD were validated by MR and were defined as candidate key genes.

3.4 LPL, IGFBP3, and APOD were identified as key genes

In order to evaluate the diagnostic value of candidate key gene therapy for DN, ROC curves were drawn in GSE96804 and GSE30528. LPL, IGFBP3, and APOD with AUC values > 0.7 in the two datasets indicated that these three genes have the ability to diagnose the occurrence of DN, and they were included in subsequent analyses **(Figure 4A-B)**. Meanwhile, LPL, IGFBP3, and APOD were significantly differentially expressed ($p < 0.05$), and the expression trend was consistent between these two datasets. APOD and LPL were down-regulated, while IGFPB3 was up-regulated in DN samples

(Figure 4C). Therefore, LPL, IGFBP3, and APOD were identified as key genes for the diagnosis of DN.

3.5 LPL, IGFBP3, and APOD were co-enriched in 26 pathways

To investigate the biological roles and pathways linked to the key genes, enrichment analysis was conducted ($p < 0.05$). By GSEA analysis, APOD was significantly associated with 38 pathways, such as protein secretion **(Figure 5A) (Supplementary Table 7)**. IGFBP3 was significantly associated with 37 pathways, such as allograft rejection **(Figure 5B) (Supplementary Table 8)**. LPL was significantly associated with 32 pathways, such as adipogenesis **(Figure 5C) (Supplementary Table 9)**. Notably, LPL, IGFBP3, and APOD were all enriched in 26 common pathways such as oxidative phosphorylation, epithelial-mesenchymal transition, heme metabolism, fatty acid metabolism, and so on **(Supplementary Table 10)**. The pathways co-enriched by these key genes deserve further exploration. It was very likely that LPL, IGFBP3, and APOD affect DN occurrence through these pathways.

3.6 LPL, IGFBP3, and APOD shared functional similarities with 20 genes

The results of chromosomal mapping of key genes showed that APOD, IGFBP3, and LPL were distributed on chromosomes 3, 7, and 8, respectively **(Figure 6A)**. Then, functional similarity analysis was conducted to identify genes with similar functions to key genes. GeneMANIA analysis revealed 20 genes that interact with LPL, IGFBP3, and APOD, such as KLK3, GPIHBP1, and others. These genes played important roles in regulatory pathways and protein interaction networks and may be associated with specific biological functions or disease mechanisms **(Figure 6B)**.

3.7 Regulatory network of LPL, IGFBP3, and APOD was performed

According to the database prediction, a total of 19 miRNAs were significantly related to LPL and IGFBP3, and 21 lncRNAs were related to 9 miRNAs. In the lncRNA-miRNA-mRNA network, MIR497HG regulated IGFBP3 by regulating hsa-miR-19a-3p. NEAT1 regulated LPL by regulating hsa-miR-29a-3p **(Figure 7A)**. All miRNAs and lncRNAs were shown in **Supplementary Table 11.** The database predicted TF of key genes to obtain the mRNA-TF relationship pair. A total of 15 TFs, such as AR and HDAC1, corresponded to IGFBP3, seven TFs, such as NFKB1 and RELA, corresponded to LPL, and only NOTCH3 corresponded to APOD. IGFBP3 and LPL were co-regulated by two TFs, including SP3 and SP1 **(Figure 7B)**. These regulatory networks for key genes also provide a reference for the molecular mechanism of DN occurrence.

3.8 LPL, IGFBP3, and APOD had good binding ability with active components

Based on the corresponding relationship between the active ingredients in the previous step and the key

genes, molecular docking was performed. After screening, each of the three key genes was matched to an active ingredient. The findings indicated that the binding energy was -6.1 kcal/mol between APOD and baicalein, -6.5 kcal/mol between LPL and oleic acid, as well as -7.5 kcal/mol between IGFBP3 and quercetin **(Table 5)**. The figure illustrates the interaction between proteins and small molecules **(Figure 8A-C)**. This indicated that the active ingredients of the drug had a good binding ability to the key genes, and the key genes had the potential to be used as drug therapeutic targets.

3.9 RT-qPCR validation of APOD, IGFBP3, and LPL

To verify the differential expression of the core key genes (LPL, IGFBP3, APOD) and the interventional effect of the XZTL group, reverse transcription quantitative RT-qPCR was performed to detect the relative expression levels of these genes in the control group, DN group, and XZTL group. The results showed that compared with the control group, the relative expression levels of LPL ($P<0.01$) and APOD ($P<0.05$) were significantly downregulated in the DN group, while that of IGFBP3 was markedly upregulated ($P<0.01$). These results were completely consistent with the expression trends observed in the GSE96804 and GSE30528 datasets, validating the authenticity of the differential expression of the core key genes. Compared with the DN group, the XZTL group exhibited a significant regulatory effect on gene expression: the relative expression levels of LPL and APOD were notably increased ($P<0.01$) and were closer to those of the control group, whereas the relative expression level of IGFBP3 was significantly decreased ($P<0.01$). No statistically significant differences were observed in the relative expression levels of the three aforementioned genes between the XZTL group and the control group ($P>0.05$). **(Figure 9)**

4. Discussion

DN is a major microvascular complication of diabetes with complex pathogenesis involving genetic susceptibility, metabolic disturbance, oxidative stress and inflammation, while accurate diagnostic biomarkers and targeted therapies remain lacking clinically (H. Zhang et al., 2025). XZTL is a Chinese herbal formula based on the TCM theory of qi-yin deficiency and collateral stasis, which improves renal function in DN patients via replenishing qi and nourishing yin, resolving stagnation and activating blood circulation, with confirmed efficacy in early DN (F.-L. Wang et al., 2012). Using network pharmacology and bioinformatics, we identified LPL, IGFBP3 and APOD as hub genes from 2693 differentially expressed genes; these genes were enriched in 26 key pathways, including oxidative

phosphorylation, epithelial-mesenchymal transition, and fatty acid metabolism, contributing to DN progression by regulating energy metabolism and renal fibrosis. Mendelian randomization verified that downregulated LPL and APOD were protective, while elevated IGFBP3 increased DN risk, establishing a causal association. RT-qPCR showed XZTL significantly normalized the abnormal expression of these three genes, and molecular docking revealed that its main active components (baicalein, quercetin, oleic acid) exhibited strong binding affinity (binding energy < −6 kcal/mol). This study elucidates the causal roles of LPL, IGFBP3, and APOD in DN and the mechanism of XZTL, providing experimental evidence for diagnostic biomarkers (all AUC > 0.7) and targeted therapeutic strategies for DN.

4.1 Screening Logic and Reliability Validation of Core Key Genes

First, transcriptome data analysis was performed in this study to identify 2693 differentially expressed genes (DEGs) between the DN and control groups. These DEGs were significantly enriched in biological pathways, including small molecule catabolism and fatty acid degradation, which were highly consistent with the core pathological features of metabolic disturbance and dysregulated lipid metabolism in DN. Furthermore, a cross-analysis of the intersection of DEGs, disease target genes, and drug target genes was conducted to pinpoint 29 candidate genes. Notably, these candidate genes were enriched in the oxidative stress response pathway and the pathway of fluid shear stress and atherosclerosis, both of which represent critical pathological processes underlying the initiation and progression of DN(Ma et al., 2021), thus verifying the functional relevance and disease specificity of the identified candidate genes.

4.2 Correlation of Biological Functions of Core Key Genes with the Pathogenesis of Diabetic Nephropathy

4.2.1 IGFBP3: A Risk Factor for DN Onset and Its Regulatory Pathways

IGFBP3, the most abundant IGFBP family member, regulates IGF-1 activity via binding/half-life modulation (mediating proliferation, apoptosis, metabolism) and modulates fibrosis/inflammation independently of IGF-1. The IGF-IGFBP axis is critical in DN(Oh, 2012). Here, IGFBP3 was significantly upregulated in DN samples, and MR analysis confirmed it as a DN risk factor. Enrichment analysis linked IGFBP3 to allograft rejection and oxidative phosphorylation; disrupted oxidative

phosphorylation-induced mitochondrial dysfunction exacerbates oxidative stress-mediated renal injury, a key mechanism of IGFBP3-driven DN (Higgins & Coughlan, 2014). Regulatory network analysis showed IGFBP3 is regulated by the MIR497HG/hsa-miR-19a-3p axis and targeted by transcription factors (AR, HDAC1, SP3, SP1), with dysregulation of these regulators (e.g., upregulated HDAC1 (Noh et al., 2009), downregulated miR-19a-3p (Zhou et al., 2018)) synergistically promoting IGFBP3 overexpression. RT-qPCR validated IGFBP3 upregulation in DN models, and XZTL intervention significantly normalized its expression, highlighting IGFBP3 as a promising therapeutic target of XZTL with clinical translational value.

4.2.2 APOD and LPL: Regulatory Roles in the Homeostasis of Lipid Metabolism

Apo-D, encoded by the APOD gene and belonging to the lipocalin superfamily, participates in lipid transport and cholesterol homeostasis as an HDL component interacting with LCAT(Flores et al., 2019). APOD serves as a biomarker for acute renal transplant rejection (Dlouha et al., 2021), and our MR analysis identified it as a risk factor for DN, despite its downregulation in DN samples. We propose that genetically higher APOD expression may increase DN susceptibility (Rossi et al., 2015), while its post-disease reduction represents secondary or compensatory changes. Reduced APOD expression disrupts lipid metabolism, promotes renal lipid deposition, inflammation, and fibrosis (Han et al., 2024), aggravating renal injury. Regulatory network analysis showed APOD is exclusively regulated by transcription factor NOTCH3. XZTL significantly upregulated APOD, suggesting restoration of lipid homeostasis as one mechanism underlying its renoprotective effects in DN, although the causal role and stage-specific function of APOD in DN require further validation.

The LPL gene encodes lipoprotein lipase (LPL), an enzyme expressed in the heart, muscle and adipose tissues(Knapp et al., 2023). LPL exerts dual functions as a triglyceride hydrolase and a ligand/bridging factor, and is essential for receptor-mediated lipoprotein uptake. As a rate-limiting enzyme in lipid metabolism, it primarily catalyzes the hydrolysis of triglycerides in the core of chylomicrons and very-low-density lipoproteins (VLDL) into free fatty acids and monoglycerides(Talmud et al., 1998). The LPL gene has multiple polymorphisms that are closely associated with the development of dyslipidemias including hyperlipidemia and hypertriglyceridemia. Severe LPL gene mutations can cause lipoprotein lipase deficiency, thereby leading to type I hyperlipoproteinemia(Ng et al., 2006). Reduced LPL activity has been observed in patients with DN. Our study identified LPL as a protective

factor for DN, with significantly decreased expression in DN samples—consistent with previous reports of reduced LPL activity in DN patients (Kashiwazaki et al., 1998). Downregulated LPL increases plasma triglyceride levels, exacerbates renal lipid deposition, oxidative stress, and fibrosis (Pei et al., 2020), which was confirmed by RT-qPCR in DN models. Enrichment analysis linked LPL to adipogenesis and, together with IGFBP3 and APOD, to pathways including oxidative phosphorylation and fatty acid metabolism. Regulatory network analysis showed LPL is regulated by the NEAT1/hsa-miR-29a-3p axis and targeted by transcription factors (NFKB1, RELA, SP3, SP1); notably, SP3 and SP1 co-regulate both LPL and IGFBP3, suggesting synergistic transcriptional regulation. XZTL significantly upregulated LPL expression, indicating its renoprotective effects may involve restoring LPL-mediated lipid metabolism. Collectively, these three hub genes likely contribute to DN progression via coordinated regulation of lipid and energy metabolism, and XZTL's simultaneous normalization of their aberrant expression provides a molecular basis for its multi-targeted therapeutic mechanism in DN.

4.3 Clinical Translational Value and Drug Targeting Potential of Core Key Genes

The constructed drug-active component-core gene network reveals the multi-target mechanism of XZTL against diabetic nephropathy (DN). Network analysis showed that seven herbs act on 29 candidate genes including IGFBP3, APOD, and LPL via 150 bioactive ingredients, embodying the multi-component, multi-target, multi-pathway synergy of traditional Chinese medicine formulas. Molecular docking verified strong binding affinities with binding energies < -6 kcal/mol: quercetin-IGFBP3 (-7.5 kcal/mol), baicalein-APOD (-6.1 kcal/mol), and oleic acid-LPL (-6.5 kcal/mol). Quercetin, a flavonoid with known lipid-regulating, antioxidant, and renoprotective activities(Chen et al., 2022) , may attenuate oxidative phosphorylation disorder and renal fibrosis by inhibiting IGFBP3 overexpression. Baicalein, a major antioxidant, anti-inflammatory, and antifibrotic component (W. Wang et al., 2015), may protect the kidney via targeting APOD to modulate lipid metabolism and oxidative stress. Oleic acid improves lipid profiles and lowers triglycerides (Listenberger et al., 2003), and may enhance LPL-mediated lipid clearance to reduce renal lipid accumulation. Notably, IGFBP3, APOD, and LPL are co-enriched in oxidative phosphorylation, fatty acid metabolism, and epithelial-mesenchymal transition, suggesting XZTL acts through coordinated regulation of these pathways. Quercetin inhibits IGFBP3 to restore oxidative phosphorylation, while

oleic acid activates LPL and baicalein regulates APOD to rebalance lipid metabolism, jointly reducing renal oxidative stress, lipid deposition, and fibrosis. This multi-component, multi-target, multi-pathway synergy highlights the advantage of XZTL and provides a scientific basis for its clinical application in DN.

In addition, the ROC curve analysis showed that the AUC values of the three core genes all exceeded 0.7, with their expression levels significantly altered in DN samples, indicating their potential as novel biomarkers for DN diagnosis. Compared with traditional indicators such as the urinary albumin-to-creatinine ratio (UACR), genetic biomarkers offer higher specificity and sensitivity,and the combined detection of the three genes may further improve diagnostic efficacy, thus providing a novel technical approach for the early screening and disease monitoring of DN.

4.4 Study Limitations and Future Perspectives

This study has certain limitations. First, CAV1 was excluded from Mendelian randomization (MR) analysis due to poor single nucleotide polymorphism (SNP) distribution, which may have led to the omission of potential key genes. In future research, expanding the sample size or using multicenter data for further validation is warranted. Second, the construction of the molecular regulatory network was based on database predictions, and the specific regulatory mechanisms underlying some predicted regulatory relationships need to be elucidated by subsequent cellular and animal experiments. Third, this study did not explore the specific regulatory patterns of the core gene co-enriched pathways (e.g., oxidative phosphorylation, epithelial-mesenchymal transition), and future studies can clarify the molecular mechanisms by which core genes regulate DN progression through these pathways using techniques such as gene silencing and overexpression.

Despite the aforementioned limitations, this study identified LPL, IGFBP3 and APOD as the core key genes of DN through multi-dimensional analyses, and clarified their diagnostic value, regulatory networks and drug targeting potential, thereby providing novel insights into the mechanistic investigation and clinical translation of DN. Building on the findings of this study, future research can focus on the development of novel drugs targeting these core genes or the construction of a multi-gene combined diagnostic model, which will offer more robust support for the precise prevention and treatment of DN.

Data Availability Statement

All data supporting this study are available from the following databases: GEO/NCBI (https://www.ncbi.nlm.nih.gov), IEU OpenGWAS (https://gwas.mrcieu.ac.uk), TCMSP (https://tcmsp.91medicine.cn/#/home), UniProtKB (https://www.uniprot.org/uniprot), GeneCards (https://www.genecards.org), TTD (http://db.idrblab.net/ttd), GeneMANIA (https://genemania.org), DIANA Tools (http://diana.imis.athena-innovation.gr/DianaTools), miRDB (https://mirdb.org), ENCORI/starBase (https://rnasysu.com/encori), miRNet (https://www.mirnet.ca), RCSB PDB (https://www.rcsb.org), PubChem Compound (https://www.ncbi.nlm.nih.gov/pccompound), and CB-Dock2 (https://cadd.labshare.cn/cb-dock2).

Acknowledgments

This work was financially supported by the National Natural Science Foundation of China (NSFC, Grant No. 82274504). The authors sincerely acknowledge the foundation for its crucial financial and resource support, which enabled the smooth implementation of the research, including experimental materials procurement, data collection, and analytical equipment usage.

We would like to express our profound gratitude to all members of the research team who made invaluable contributions to this manuscript but do not meet the criteria for authorship. Their meticulous work laid a solid foundation for the completion of this study. We also thank team members for the constructive discussions and intellectual exchanges during the research process, as well as their selfless sharing of professional knowledge and technical experience, which significantly enriched the research ideas and improved the quality of the manuscript. All contributions mentioned above were included with the explicit permission of the contributors.

Conflict of Interest Statement

All authors declare that there are no commercial interests, personal relationships, or other potential conflicts of interest that could compromise the objectivity of this study. No author has any competing financial interests to disclose.

Consent to Publish declaration

Not applicable.

Ethics Declaration

The present study was approved by the Institutional Animal Care and Use Committee (IACUC) of Hebei Provincial Hospital of Traditional Chinese Medicine (Approval No.: IACUC-HPHCM-2024017). All animal experiments were performed in strict compliance with the Guide for the Care and Use of Laboratory Animals (NIH Publication No. 85-23, revised 1996) and the 3R principles (Replacement, Reduction, Refinement) to minimize animal suffering. The animal facility meets standard requirements for laboratory animal care and management.

Consent to Participate declarations

Not applicable.

Author Contributions

Conceptualization: Zhao Liu, Moxixuan Liu;

Methodology: Zhao Liu, Moxixuan Liu, Haina Wu;

Validation: Xiaona Wei, Hui Gao;

Formal Analysis: Zhao Liu, Moxixuan Liu;

Investigation: Yun Ma, Xinai Wang;

Data Curation: Jinmei Zheng, Jing Liang;

Writing – Original Draft: All authors;

Writing – Review & Editing: All authors;

Visualization: Ying Zhang;

Supervision: Zhiqiang Chen;

Project Administration: Zhiqiang Chen;

Funding Acquisition: Zhiqiang Chen.

References

Chen, Y.-Q., Chen, H.-Y., Tang, Q.-Q., Li, Y.-F., Liu, X.-S., Lu, F.-H., & Gu, Y.-Y. (2022). Protective effect of quercetin on kidney diseases: From chemistry to herbal medicines. *Frontiers in Pharmacology*, *13*, 968226. https://doi.org/10.3389/fphar.2022.968226

Dai, Z., Xu, W., Ding, R., Peng, X., Shen, X., Song, J., Du, P., Wang, Z., & Liu, Y. (2023). Two-sample Mendelian randomization analysis evaluates causal associations between inflammatory bowel disease and osteoporosis. *Frontiers in Public Health*, *11*, 1151837. https://doi.org/10.3389/fpubh.2023.1151837

Dlouha, L., Pelikanova, T., Veleba, J., Adamkova, V., Lanska, V., Sosna, T., Pacal, L., Kankova, K., & Hubacek, J. A. (2021). The APOE4 allele is associated with a decreased risk of retinopathy in type 2 diabetics. *Molecular Biology Reports*, *48*(8), 5873–5879. https://doi.org/10.1007/s11033-021-06581-w

Dong, Q., Chen, D., Zhang, Y., Xu, Y., Yan, L., & Jiang, J. (2023). Constipation and cardiovascular disease: A two-sample Mendelian randomization analysis. *Frontiers in Cardiovascular Medicine*, *10*, 1080982. https://doi.org/10.3389/fcvm.2023.1080982

Dwivedi, S., & Sikarwar, M. S. (2025). Diabetic Nephropathy: Pathogenesis, Mechanisms, and Therapeutic Strategies. *Hormone and Metabolic Research*, *57*(01), 7–17. https://doi.org/10.1055/a-2435-8264

Ference, B. A., Holmes, M. V., & Smith, G. D. (2021). Using Mendelian Randomization to Improve the Design of Randomized Trials. *Cold Spring Harbor Perspectives in Medicine*, *11*(7), a040980. https://doi.org/10.1101/cshperspect.a040980

Flores, R., Jin, X., Chang, J., Zhang, C., Cogan, D. G., Schaefer, E. J., & Kruth, H. S. (2019). LCAT, ApoD, and ApoA1 Expression and Review of Cholesterol Deposition in the Cornea. *Biomolecules*, *9*(12), 785. https://doi.org/10.3390/biom9120785

Gan, T., Hu, J., Liu, W., Li, C., Xu, Q., Wang, Y., Lu, S., Aledan, A. K. O., Wang, Y., & Wang, Z. (2023). Causal Association Between Anemia and Cardiovascular Disease: A 2-Sample Bidirectional Mendelian Randomization Study. *Journal of the American Heart Association*, *12*(12), e029689. https://doi.org/10.1161/JAHA.123.029689

Gu, Z., Eils, R., & Schlesner, M. (2016). Complex heatmaps reveal patterns and correlations in multidimensional genomic data. *Bioinformatics*, *32*(18), 2847–2849. https://doi.org/10.1093/bioinformatics/btw313

Han, Y.-Z., Du, B.-X., Zhu, X.-Y., Wang, Y.-Z.-Y., Zheng, H.-J., & Liu, W.-J. (2024). Lipid metabolism disorder in diabetic kidney disease. *Frontiers in Endocrinology*, *15*, 1336402. https://doi.org/10.3389/fendo.2024.1336402

Hemani, G., Zheng, J., Elsworth, B., Wade, K. H., Haberland, V., Baird, D., Laurin, C., Burgess, S., Bowden, J., Langdon, R., Tan, V. Y., Yarmolinsky, J., Shihab, H. A., Timpson, N. J., Evans, D. M., Relton, C., Martin, R. M., Davey Smith, G., Gaunt, T. R., & Haycock, P. C. (2018). The MR-Base platform supports systematic causal inference across the human phenome. *eLife*, *7*, e34408. https://doi.org/10.7554/eLife.34408

Higgins, G. C., & Coughlan, M. T. (2014). Mitochondrial dysfunction and mitophagy: The beginning and end to diabetic nephropathy? *British Journal of Pharmacology*, *171*(8), 1917–1942. https://doi.org/10.1111/bph.12503

Hsu, Y.-C., Shih, Y.-H., Ho, C., Liu, C.-C., Liaw, C.-C., Lin, H.-Y., & Lin, C.-L. (2024). Ethyl Acetate Fractions of Salvia miltiorrhiza Bunge (Danshen) Crude Extract Modulate Fibrotic Signals to Ameliorate Diabetic Kidney Injury. *International Journal of Molecular Sciences*, *25*(16), 8986. https://doi.org/10.3390/ijms25168986

Kashiwazaki, K., Hirano, T., Yoshino, G., Kurokawa, M., Tajima, H., & Adachi, M. (1998). Decreased release of lipoprotein lipase is associated with vascular endothelial damage in NIDDM patients with microalbuminuria. *Diabetes Care*, *21*(11), 2016–2020. https://doi.org/10.2337/diacare.21.11.2016

Kim, Y. K., Ning, X., Munir, K. M., & Davis, S. N. (2022). Emerging drugs for the treatment of diabetic nephropathy. *Expert Opinion on Emerging Drugs*, *27*(4), 417–430. https://doi.org/10.1080/14728214.2022.2155632

Knapp, M., Łukaszuk, B., Lisowska, A., Hirnle, T., Górski, J., Chabowski, A., & Mikłosz, A. (2023). Multivessel Coronary Artery Disease Complicated by Diabetes Mellitus Has a Relatively Small Effect on Endothelial and Lipoprotein Lipases Expression in the Human Atrial Myocardium and Coronary Perivascular Adipose Tissue. *International Journal of Molecular Sciences*, *24*(17), 13552. https://doi.org/10.3390/ijms241713552

Li, B., Zhao, X., Xie, W., Hong, Z., & Zhang, Y. (2023). Integrative analyses of biomarkers and pathways for diabetic nephropathy. *Frontiers in Genetics*, *14*, 1128136. https://doi.org/10.3389/fgene.2023.1128136

Li, N., Wang, Y., Wei, P., Min, Y., Yu, M., Zhou, G., Yuan, G., Sun, J., Dai, H., Zhou, E., He, W., Sheng,

M., Gao, K., Zheng, M., Sun, W., Zhou, D., & Zhang, L. (2023). Causal Effects of Specific Gut Microbiota on Chronic Kidney Diseases and Renal Function—A Two-Sample Mendelian Randomization Study. *Nutrients*, *15*(2), 360. https://doi.org/10.3390/nu15020360

Listenberger, L. L., Han, X., Lewis, S. E., Cases, S., Farese, R. V., Ory, D. S., & Schaffer, J. E. (2003). Triglyceride accumulation protects against fatty acid-induced lipotoxicity. *Proceedings of the National Academy of Sciences of the United States of America*, *100*(6), 3077–3082. https://doi.org/10.1073/pnas.0630588100

Liu, J., Tang, R., Zheng, J., & Luo, K. (2024). Targeting ferroptosis reveals a new strategy for breast cancer treatment: A bibliometric study. *Discover Oncology*, *15*(1), 679. https://doi.org/10.1007/s12672-024-01569-x

Liu, X.-J., Hu, X.-K., Yang, H., Gui, L.-M., Cai, Z.-X., Qi, M.-S., & Dai, C.-M. (2022). A Review of Traditional Chinese Medicine on Treatment of Diabetic Nephropathy and the Involved Mechanisms. *The American Journal of Chinese Medicine*, *50*(07), 1739–1779. https://doi.org/10.1142/S0192415X22500744

Liu, Z., Wang, H., Yang, Z., Lu, Y., & Zou, C. (2023). Causal associations between type 1 diabetes mellitus and cardiovascular diseases: A Mendelian randomization study. *Cardiovascular Diabetology*, *22*(1), 236. https://doi.org/10.1186/s12933-023-01974-6

Ma, L., Wu, F., Shao, Q., Chen, G., Xu, L., & Lu, F. (2021). Baicalin Alleviates Oxidative Stress and Inflammation in Diabetic Nephropathy via Nrf2 and MAPK Signaling Pathway. *Drug Design, Development and Therapy*, *Volume 15*, 3207–3221. https://doi.org/10.2147/DDDT.S319260

Mounier, N., & Kutalik, Z. (2023). Bias correction for inverse variance weighting Mendelian randomization. *Genetic Epidemiology*, *47*(4), 314–331. https://doi.org/10.1002/gepi.22522

Ng, M., Baum, L., So, W., Lam, V., Wang, Y., Poon, E., Tomlinson, B., Cheng, S., Lindpaintner, K., & Chan, J. (2006). Association of lipoprotein lipase S447X, apolipoprotein E exon 4, and apoC3 −455T>C polymorphisms on the susceptibility to diabetic nephropathy. *Clinical Genetics*, *70*(1), 20–28. https://doi.org/10.1111/j.1399-0004.2006.00628.x

Noh, H., Oh, E. Y., Seo, J. Y., Yu, M. R., Kim, Y. O., Ha, H., & Lee, H. B. (2009). Histone deacetylase-2 is a key regulator of diabetes- and transforming growth factor-beta1-induced renal injury. *American Journal of Physiology. Renal Physiology*, *297*(3), F729-739. https://doi.org/10.1152/ajprenal.00086.2009

Oh, Y. (2012). The insulin-like growth factor system in chronic kidney disease: Pathophysiology and therapeutic opportunities. *Kidney Research and Clinical Practice*, *31*(1), 26–37. https://doi.org/10.1016/j.krcp.2011.12.005

Pei, K., Gui, T., Li, C., Zhang, Q., Feng, H., Li, Y., Wu, J., & Gai, Z. (2020). Recent Progress on Lipid Intake and Chronic Kidney Disease. *BioMed Research International*, *2020*, 3680397. https://doi.org/10.1155/2020/3680397

Qi, X.-Y., Peng, G.-C., Han, Q.-T., Yan, J., Chen, L.-Z., Wang, T., Xu, L.-T., Liu, M.-J., Xu, Z.-P., Wang, X.-N., & Shen, T. (2024). Phthalides from the rhizome of Ligusticum chuanxiong Hort. Attenuate diabetic nephropathy in mice. *Journal of Ethnopharmacology*, *319*, 117247. https://doi.org/10.1016/j.jep.2023.117247

Reutens, A. T., & Atkins, R. C. (2011). Epidemiology of Diabetic Nephropathy. In K. N. Lai & S. C. W. Tang (Eds), *Contributions to Nephrology* (Vol. 170, pp. 1–7). S. Karger AG. https://doi.org/10.1159/000324934

Ritchie, M. E., Phipson, B., Wu, D., Hu, Y., Law, C. W., Shi, W., & Smyth, G. K. (2015). Limma powers differential expression analyses for RNA-sequencing and microarray studies. *Nucleic Acids Research*, *43*(7), e47–e47. https://doi.org/10.1093/nar/gkv007

Robin, X., Turck, N., Hainard, A., Tiberti, N., Lisacek, F., Sanchez, J.-C., & Müller, M. (2011). pROC: An open-source package for R and S+ to analyze and compare ROC curves. *BMC Bioinformatics*, *12*(1), 77. https://doi.org/10.1186/1471-2105-12-77

Rossi, A., Kontarakis, Z., Gerri, C., Nolte, H., Hölper, S., Krüger, M., & Stainier, D. Y. R. (2015). Genetic compensation induced by deleterious mutations but not gene knockdowns. *Nature*, *524*(7564), 230–233. https://doi.org/10.1038/nature14580

Shannon, P., Markiel, A., Ozier, O., Baliga, N. S., Wang, J. T., Ramage, D., Amin, N., Schwikowski, B., & Ideker, T. (2003). Cytoscape: A Software Environment for Integrated Models of Biomolecular Interaction Networks. *Genome Research*, *13*(11), 2498–2504. https://doi.org/10.1101/gr.1239303

Sui, Y., Liu, W., Tian, W., Li, X.-Q., & Cao, W. (2019). A branched arabinoglucan from Angelica sinensis ameliorates diabetic renal damage in rats. *Phytotherapy Research: PTR*, *33*(3), 818–831. https://doi.org/10.1002/ptr.6275

Sun, L., Yang, Z., Zhao, W., Chen, Q., Bai, H., Wang, S., Yang, L., Bi, C., Shi, Y., & Liu, Y. (2022). Integrated lipidomics, transcriptomics and network pharmacology analysis to reveal the mechanisms of

Danggui Buxue Decoction in the treatment of diabetic nephropathy in type 2 diabetes mellitus. *Journal of Ethnopharmacology*, *283*, 114699. https://doi.org/10.1016/j.jep.2021.114699

Talmud, P. J., Hall, S., Holleran, S., Ramakrishnan, R., Ginsberg, H. N., & Humphries, S. E. (1998). LPL promoter -93T/G transition influences fasting and postprandial plasma triglycerides response in African-Americans and Hispanics. *Journal of Lipid Research*, *39*(6), 1189–1196.

Wang, F.-L., Chen, Z.-Q., & Wang, Y.-H. (2012). [Clinical observation of treating early diabetic nephropathy by qi supplementing, yin nourishing, blood stasis dispersing, collateral dredging recipe]. *Zhongguo Zhong Xi Yi Jie He Za Zhi Zhongguo Zhongxiyi Jiehe Zazhi = Chinese Journal of Integrated Traditional and Western Medicine*, *32*(1), 35–38.

Wang, W., Zhou, P., Xu, C., Zhou, X., Hu, W., & Zhang, J. (2015). Baicalein attenuates renal fibrosis by inhibiting inflammation via down-regulating NF-κB and MAPK signal pathways. *Journal of Molecular Histology*, *46*(3), 283–290. https://doi.org/10.1007/s10735-015-9621-8

Wu, T., Hu, E., Xu, S., Chen, M., Guo, P., Dai, Z., Feng, T., Zhou, L., Tang, W., Zhan, L., Fu, X., Liu, S., Bo, X., & Yu, G. (2021). clusterProfiler 4.0: A universal enrichment tool for interpreting omics data. *The Innovation*, *2*(3), 100141. https://doi.org/10.1016/j.xinn.2021.100141

Xian, W., Wu, D., Liu, B., Hong, S., Huo, Z., Xiao, H., & Li, Y. (2023). Graves Disease and Inflammatory Bowel Disease: A Bidirectional Mendelian Randomization. *The Journal of Clinical Endocrinology & Metabolism*, *108*(5), 1075–1083. https://doi.org/10.1210/clinem/dgac683

Xu, J., Zhang, S., Tian, Y., Si, H., Zeng, Y., Wu, Y., Liu, Y., Li, M., Sun, K., Wu, L., & Shen, B. (2022). Genetic Causal Association between Iron Status and Osteoarthritis: A Two-Sample Mendelian Randomization. *Nutrients*, *14*(18), 3683. https://doi.org/10.3390/nu14183683

Zein, R. A., & Akhtar, H. (2025). Getting started with the graded response model: An introduction and tutorial in R. *International Journal of Psychology*, *60*(1), e13265. https://doi.org/10.1002/ijop.13265

Zhang, H., Meltzer, P., & Davis, S. (2013). RCircos: An R package for Circos 2D track plots. *BMC Bioinformatics*, *14*(1), 244. https://doi.org/10.1186/1471-2105-14-244

Zhang, H., Wang, K., Zhao, H., Qin, B., Cai, X., Wu, M., Li, J., & Wang, J. (2025). Diabetic kidney disease: From pathogenesis to multimodal therapy–current evidence and future directions. *Frontiers in Medicine*, *12*, 1631053. https://doi.org/10.3389/fmed.2025.1631053

Zhang, W., Ma, L., Zhou, Q., Gu, T., Zhang, X., & Xing, H. (2024). Therapeutic Targets for Diabetic Kidney Disease: Proteome-Wide Mendelian Randomization and Colocalization Analyses. *Diabetes*,

73(4), 618–627. https://doi.org/10.2337/db23-0564

Zhang, X., Wang, J., Xiang, S., Zhao, L., Lv, M., Duan, Y., Gao, G., Wang, P., Jie Chen, J., Xu, J., Xie, Z., & Zhang, Z. (2024). Astragaloside I from *Astragalus* Attenuates Diabetic Kidney Disease by Regulating HDAC3/Klotho/TGF- **β** 1 Loop. *The American Journal of Chinese Medicine*, *52*(06), 1795–1817. https://doi.org/10.1142/S0192415X24500708

Zhang, X.-X., Kong, J., & Yun, K. (2020). Prevalence of Diabetic Nephropathy among Patients with Type 2 Diabetes Mellitus in China: A Meta-Analysis of Observational Studies. *Journal of Diabetes Research*, *2020*, 1–11. https://doi.org/10.1155/2020/2315607

Zhao, L., Zhang, H., Li, N., Chen, J., Xu, H., Wang, Y., & Liang, Q. (2023). Network pharmacology, a promising approach to reveal the pharmacology mechanism of Chinese medicine formula. *Journal of Ethnopharmacology*, *309*, 116306. https://doi.org/10.1016/j.jep.2023.116306

Zheng, Y., Gao, W., Zhang, Q., Cheng, X., Liu, Y., Qi, Z., & Li, T. (2022). Ferroptosis and Autophagy-Related Genes in the Pathogenesis of Ischemic Cardiomyopathy. *Frontiers in Cardiovascular Medicine*, *9*, 906753. https://doi.org/10.3389/fcvm.2022.906753

Zheng, Y., & Huang, X. (2024). Identification of pyroptosis-associated miRNAs in the immunoscape and prognosis of hepatocellular carcinoma. *BMC Cancer*, *24*(1), 1513. https://doi.org/10.1186/s12885-024-13276-5

Zhou, X.-L., Xu, H., Liu, Z.-B., Wu, Q.-C., Zhu, R.-R., & Liu, J.-C. (2018). miR-21 promotes cardiac fibroblast-to-myofibroblast transformation and myocardial fibrosis by targeting Jagged1. *Journal of Cellular and Molecular Medicine*, *22*(8), 3816–3824. https://doi.org/10.1111/jcmm.13654

Figure 1. Identification and functional enrichment analysis of DEGs in DN

(A-B) Volcano plot and/or expression distribution of differentially expressed genes (DEGs) between DN and control groups. A total of 2,693 DEGs were identified, including 1,290 upregulated genes (e.g., *FN1*) and 1,403 downregulated genes (e.g., *HBA1*) in the DN group.

(C-D) GO and KEGG enrichment analyses of DEGs. A total of 1386 BPs, 105 CCs, 224 MFs, and 79 KEGG pathways were significantly enriched ($p < 0.05$). DEGs were mainly enriched in small molecule catabolic process (BP), apical part of cell (CC), sulfur compound binding (MF), and fatty acid degradation (KEGG). The top five terms by count (GO) and top five pathways by p-value (KEGG) are displayed.

Figure 2. Screening and functional analysis of candidate genes for DN

(A) Venn diagram showing 29 candidate genes obtained from the intersection of 2,693 DEGs, 4,388 disease target genes, and 488 drug target genes.

(B-C) GO and KEGG enrichment analyses of 29 candidate genes ($p < 0.05$). Candidate genes were mainly enriched in response to oxidative stress (BP), membrane raft (CC), antioxidant activity (MF), and fluid shear stress and atherosclerosis (KEGG).

(D) Disease-candidate gene-active ingredient-drug network. Seven drugs yielded 150 effective active ingredients (e.g., MOL002694) that targeted 29 candidate genes (e.g., *IGFBP3*) in DN. *PTGS1* was targeted by the most active ingredients.(E) Active ingredient-candidate gene-enriched pathway network, including 15 pathways (e.g., growth factor binding), candidate genes, and effective active ingredients.

Figure 3. Mendelian randomization (MR) analysis of candidate genes

(A-B) Scatter plots and forest plots of MR analysis based on the IVW algorithm. *IGFBP3* and *APOD* were risk factors for DN (positive slope, IVW effect > 0), while *CAV1* and *LPL* were protective factors (negative slope, IVW effect < 0).

(C) Funnel plots for MR sensitivity analysis. SNPs of *APOD*, *IGFBP3*, and *LPL* were symmetrically distributed, whereas *CAV1* showed poor symmetry and was excluded.

(D) Leave-one-out (LOO) analysis confirmed the stability and reliability of MR results for *LPL*, *IGFBP3*, and *APOD*.

Figure 4. Diagnostic value and expression of key genes in DN

(A-B) ROC curve analysis of candidate key genes in GSE96804 and GSE30528 datasets. *LPL*, *IGFBP3*, and *APOD* showed AUC > 0.7 in both datasets, indicating favorable diagnostic performance for DN.

(C) Expression levels of *LPL*, *IGFBP3*, and *APOD* in DN samples. *APOD* and *LPL* were significantly down-regulated, while *IGFBP3* was significantly up-regulated ($p < 0.05$), with consistent trends in both datasets.

Figure 5. GSEA enrichment analysis of key genes in DN

(A-C) GSEA results showing top enriched pathways for *APOD*, *IGFBP3*, and *LPL*, respectively. *APOD* was significantly associated with 38 pathways (e.g., protein secretion); *IGFBP3* with 37 pathways (e.g., allograft rejection); *LPL* with 32 pathways (e.g., adipogenesis). All three genes were co-enriched in 26 common pathways including oxidative phosphorylation, epithelial-mesenchymal transition, heme metabolism, and fatty acid metabolism.

Figure 6. Chromosomal localization and functional interaction of key genes

(A) Chromosomal mapping of key genes. *APOD*, *IGFBP3*, and *LPL* were located on chromosomes 3, 7, and 8, respectively.

(B) GeneMANIA functional interaction network showing 20 genes interacting with *LPL*, *IGFBP3*, and *APOD* (e.g., *KLK3*, *GPIHBP1*).

Figure 7. Regulatory networks of key genes in DN

(A) lncRNA-miRNA-mRNA regulatory network. A total of 19 miRNAs were associated with *LPL* and *IGFBP3*, and 21 lncRNAs were linked to 9 miRNAs. *MIR497HG* regulated *IGFBP3* via hsa-miR-19a-3p; *NEAT1* regulated *LPL* via hsa-miR-29a-3p.

(B) mRNA-transcription factor (TF) network. Fifteen TFs (e.g., AR, HDAC1) targeted *IGFBP3*; seven TFs (e.g., NFKB1, RELA) targeted *LPL*; only NOTCH3 targeted *APOD*. *IGFBP3* and *LPL* were co-regulated by SP3 and SP1.

Figure 8. Molecular docking of key genes with active ingredients

(A-C) Molecular docking diagrams showing the binding modes and interactions between key genes and corresponding active ingredients. Binding energies were −6.1 kcal/mol (APOD-baicalein), −6.5 kcal/mol (LPL-oleic acid), and −7.5 kcal/mol (IGFBP3-quercetin), indicating strong binding affinity.

Figure 9. Compared with the DN group, the XZTL group exhibited a significant regulatory effect on gene expression

The relative expression levels of LPL and APOD were notably increased ($P<0.01$) and were closer to those of the control group, whereas the relative expression level of IGFBP3 was significantly decreased ($P<0.01$). No statistically significant differences were observed in the relative expression levels of the three aforementioned genes between the XZTL group and the control group ($P>0.05$).

Table 1. MR analysis results of candidate genes associated with DN (IVW algorithm)

Mendelian randomization (MR) analysis results of candidate genes associated with DN based on the IVW algorithm. eQTL data of 18 candidate genes were screened, and IGFBP3, APOD, CAV1, and LPL were significantly associated with DN ($p < 0.05$).

Table 2. Heterogeneity test results of MR analysis for key genes

Heterogeneity test results of MR analysis for key genes. The p-values of heterogeneity test for LPL, IGFBP3, and APOD were all > 0.05, indicating no significant heterogeneity.

Table 3. Horizontal pleiotropy test results of MR analysis for key genes

Horizontal pleiotropy test results of MR analysis for key genes. The p-values of horizontal pleiotropy test for LPL, IGFBP3, and APOD were all > 0.05, indicating no significant horizontal pleiotropy.

Table 4. Steiger test results of key genes

Steiger test results of key genes. The Steiger test results for LPL, IGFBP3, and APOD were all TRUE (p), verifying that the analysis results were not affected by reverse causality.

Table 5. Molecular docking results of key genes with active ingredients

Molecular docking results of key genes with active ingredients. The binding energies and interactions between APOD and baicalein, LPL and oleic acid, IGFBP3 and quercetin are shown. The binding energies were −6.1 kcal/mol, −6.5 kcal/mol, and −7.5 kcal/mol, respectively, indicating strong binding affinity.

Supplementary Table 1. Full GO enrichment information of DEGs

Full GO enrichment information of differentially expressed genes (DEGs), including 1386 biological processes (BPs), 105 cellular components (CCs), and 224 molecular functions (MFs) (p).

Supplementary Table 2. Full KEGG pathway enrichment information of DEGs

Full KEGG pathway enrichment information of differentially expressed genes (DEGs), with a total of 79 significantly enriched pathways (p).

Supplementary Table 3. Predicted disease target genes

List of predicted disease target genes, including a total of 4388 disease target genes.

Supplementary Table 4. Predicted drug target genes

List of predicted drug target genes, including a total of 488 drug target genes.

Supplementary Table 5. Full GO enrichment information of candidate genes

Full GO enrichment information of candidate genes, including 1129 biological processes (BPs), 41 cellular components (CCs), and 86 molecular functions (MFs) (p 0.05).

Supplementary Table 6. Full KEGG pathway enrichment information of candidate genes

Full KEGG pathway enrichment information of candidate genes, with a total of 51 significantly enriched pathways (p 5).

Supplementary Table 7. GSEA enrichment pathways of APOD

GSEA enrichment pathway information of APOD, including 38 significantly associated pathways (e.g., protein secretion pathway).

Supplementary Table 8. GSEA enrichment pathways of IGFBP3

GSEA enrichment pathway information of IGFBP3, including 37 significantly associated pathways (e.g., allograft rejection pathway).

Supplementary Table 9. GSEA enrichment pathways of LPL

GSEA enrichment pathway information of LPL, including 32 significantly associated pathways (e.g., adipogenesis pathway).

Supplementary Table 10. Common GSEA enrichment pathways of LPL, IGFBP3, and APOD

Common GSEA enrichment pathway information of LPL, IGFBP3, and APOD, including 26 common pathways (e.g., oxidative phosphorylation, epithelial-mesenchymal transition, heme metabolism, fatty acid metabolism, etc.).

Supplementary Table 11. miRNAs and lncRNAs in the lncRNA-miRNA-mRNA regulatory network

Complete list of microRNAs (miRNAs) and long non-coding RNAs (lncRNAs) in the lncRNA-miRNA-mRNA regulatory network, including 19 miRNAs and 21 lncRNAs.

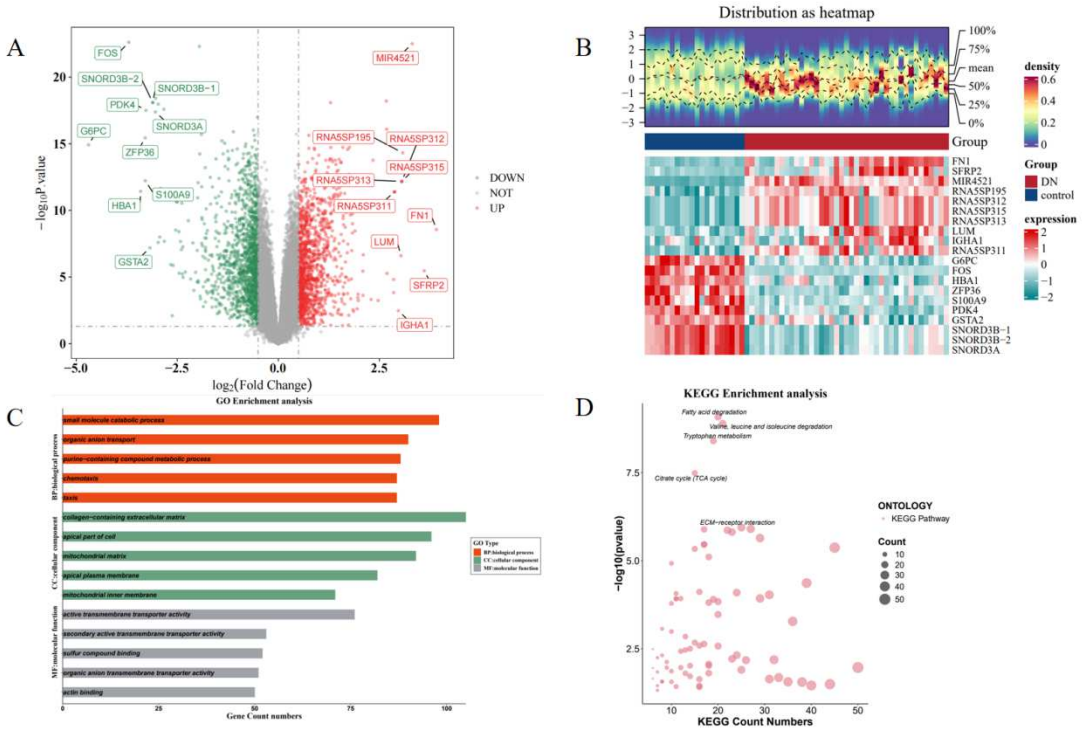

A
FOS
SNORD3B−2
SNORD3B−1
PDK4
G6PC
SNORD3A
ZFP36
S100A9
HBA1
GSTA2
MIR4521
RNA5SP195
RNA5SP312
RNA5SP315
RNA5SP313
RNA5SP311
FN1
LUM
SFRP2
IGHA1
DOWN
NOT
UP
−log10P value
log2(Fold Change)
B
Distribution as heatmap
100%
75%
mean
50%
25%
0%
density
Group
DN
control
expression
FN1
SFRP2
MIR4521
RNA5SP195
RNA5SP312
RNA5SP315
RNA5SP313
LUM
IGHA1
RNA5SP311
G6PC
FOS
HBA1
ZFP36
S100A9
PDK4
GSTA2
SNORD3B−1
SNORD3B−2
SNORD3A
C
GO Enrichment analysis
small molecule catabolic process
organic anion transport
purine−containing compound metabolic process
chemotaxis
taxis
collagen−containing extracellular matrix
apical part of cell
mitochondrial matrix
apical plasma membrane
mitochondrial inner membrane
active transmembrane transporter activity
secondary active transmembrane transporter activity
sulfur compound binding
organic anion transmembrane transporter activity
actin binding
BP:biological process
CC:cellular component
MF:molecular function
GO Type
Gene Count numbers
D
KEGG Enrichment analysis
Fatty acid degradation
Valine, leucine and isoleucine degradation
Tryptophan metabolism
Citrate cycle (TCA cycle)
ECM−receptor interaction
ONTOLOGY
KEGG Pathway
Count
−log10(pvalue)
KEGG Count Numbers

Figure 1.

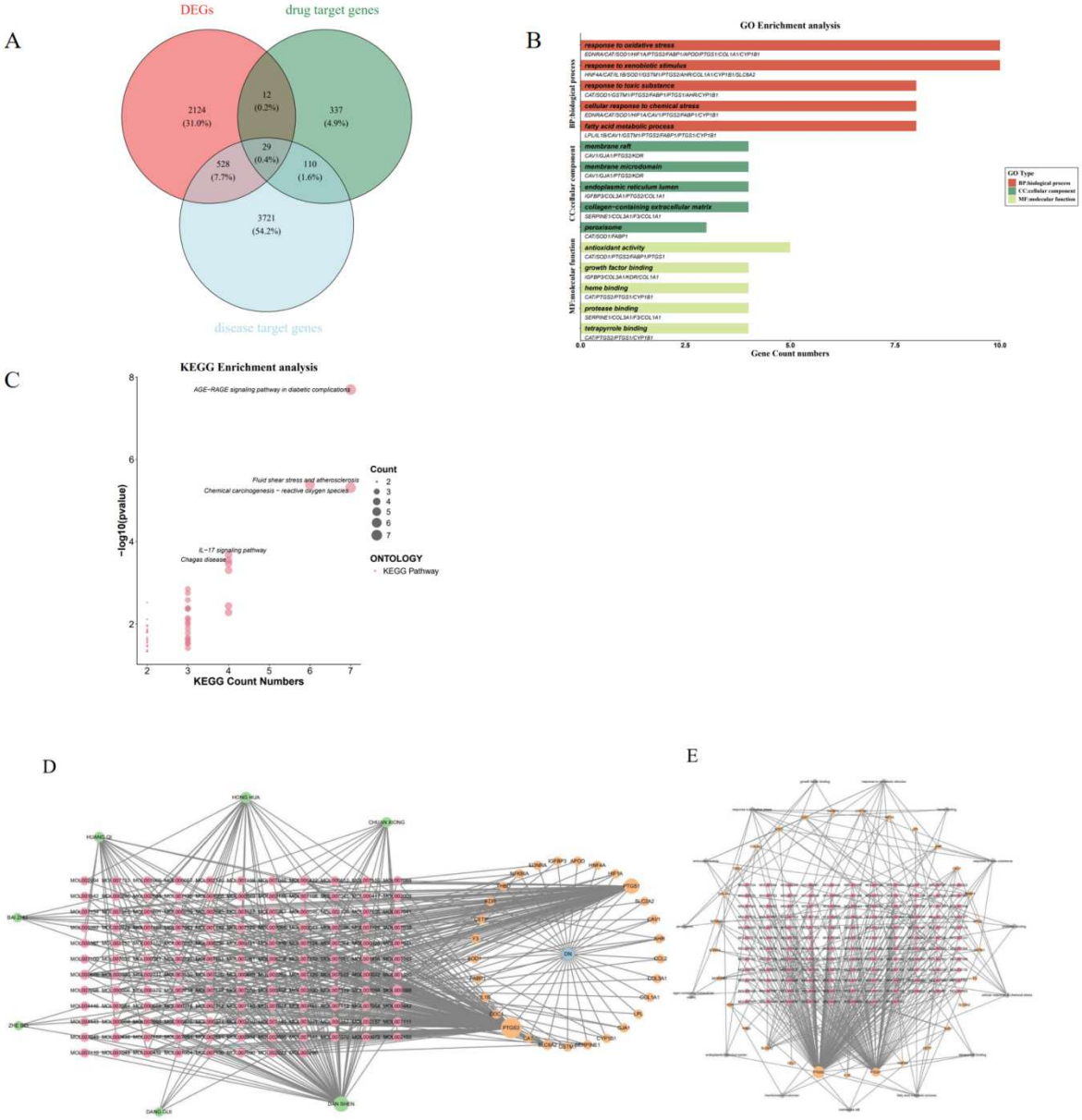
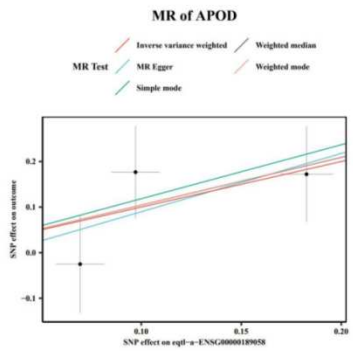
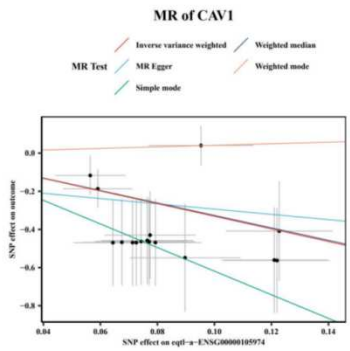

A
DEGs
drug target genes
disease target genes
2124
(31.0%)
12
(0.2%)
337
(4.9%)
29
(0.4%)
528
(7.7%)
110
(1.6%)
3721
(54.2%)
B
GO Enrichment analysis
response to oxidative stress
response to xenobiotic stimulus
response to toxic substance
cellular response to chemical stress
fatty acid metabolic process
membrane raft
membrane microdomain
endoplasmic reticulum lumen
collagen−containing extracellular matrix
peroxisome
antioxidant activity
growth factor binding
heme binding
protease binding
tetrapyrrole binding
BP:biological process
CC:cellular component
MF:molecular function
GO Type
Gene Count numbers
C
KEGG Enrichment analysis
AGE−RAGE signaling pathway in diabetic complications
Fluid shear stress and atherosclerosis
Chemical carcinogenesis − reactive oxygen species
IL−17 signaling pathway
Chagas disease
−log10(pvalue)
Count
ONTOLOGY
KEGG Pathway
KEGG Count Numbers
D
E

Figure 2.

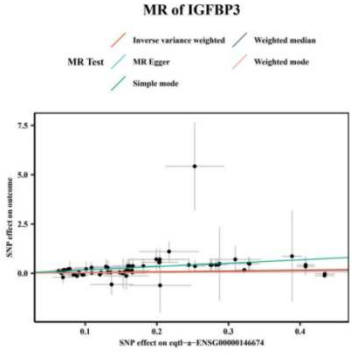
A1



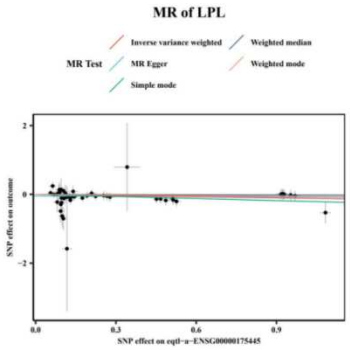
A2



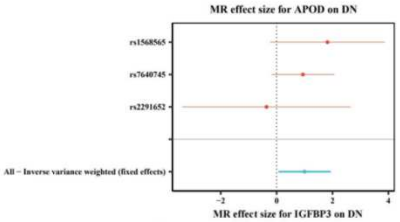
A3



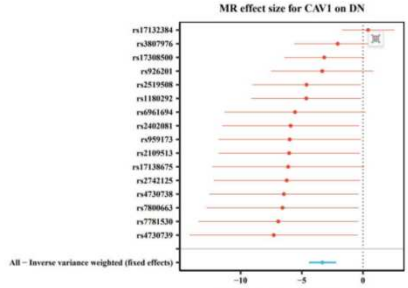
A4



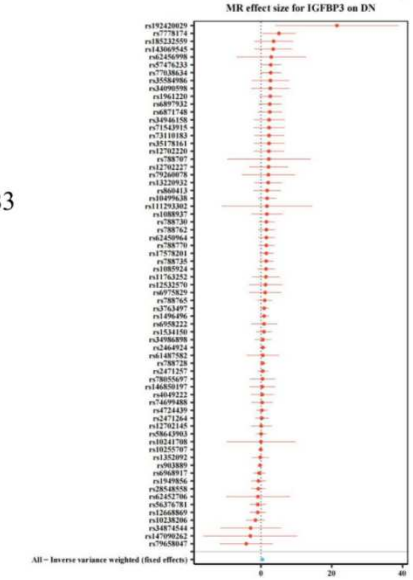
B1



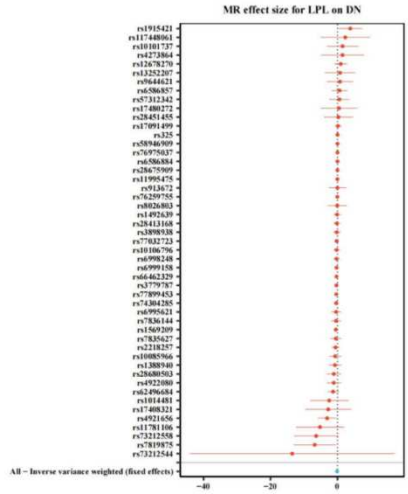
B2



B3



B4



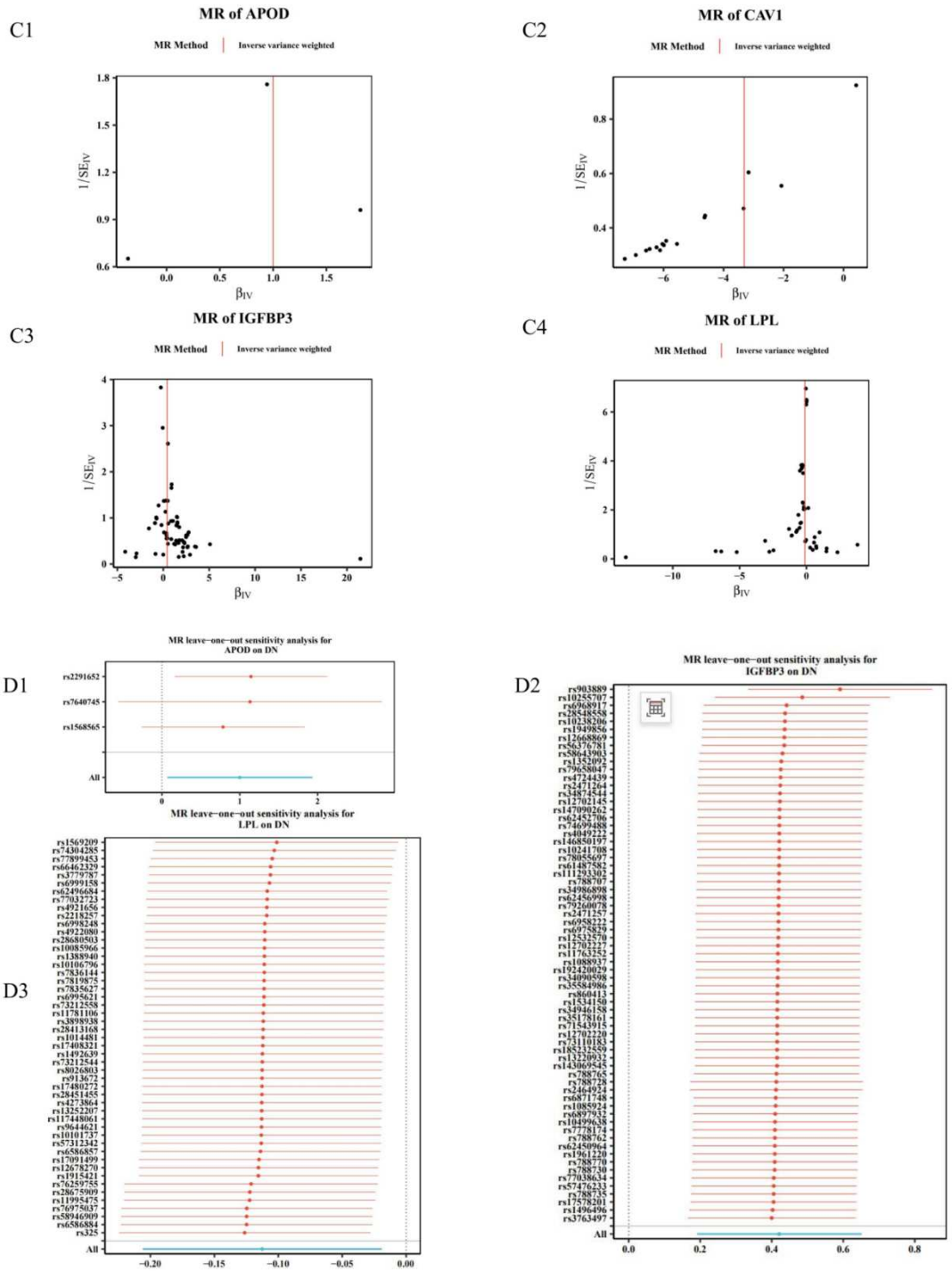

C1
MR of APOD
MR Method
Inverse variance weighted
C2
MR of CAV1
MR Method
Inverse variance weighted
C3
MR of IGFBP3
MR Method
Inverse variance weighted
C4
MR of LPL
MR Method
Inverse variance weighted
D1
MR leave−one−out sensitivity analysis for APOD on DN
D2
MR leave−one−out sensitivity analysis for IGFBP3 on DN
D3
MR leave−one−out sensitivity analysis for LPL on DN

Figure 3.

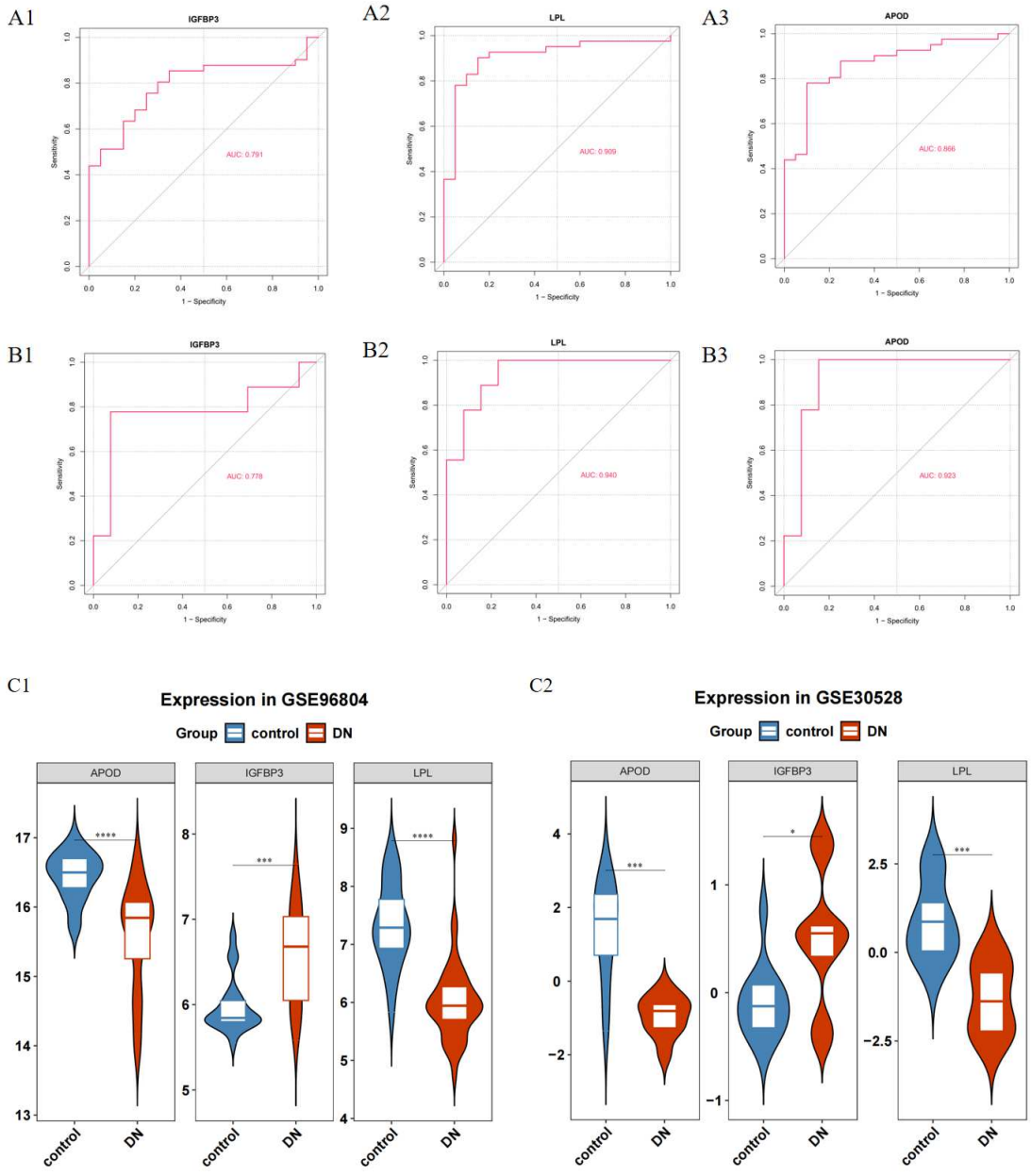

A1
IGFBP3
AUC: 0.791
A2
LPL
AUC: 0.909
A3
APOD
AUC: 0.866
B1
IGFBP3
AUC: 0.778
B2
LPL
AUC: 0.940
B3
APOD
AUC: 0.923
Sensitivity
1 − Specificity
C1
Expression in GSE96804
Group control DN
APOD
IGFBP3
LPL
****
***
****
control
DN
C2
Expression in GSE30528
Group control DN
APOD
IGFBP3
LPL
***
*
***
control
DN

Figure 4.

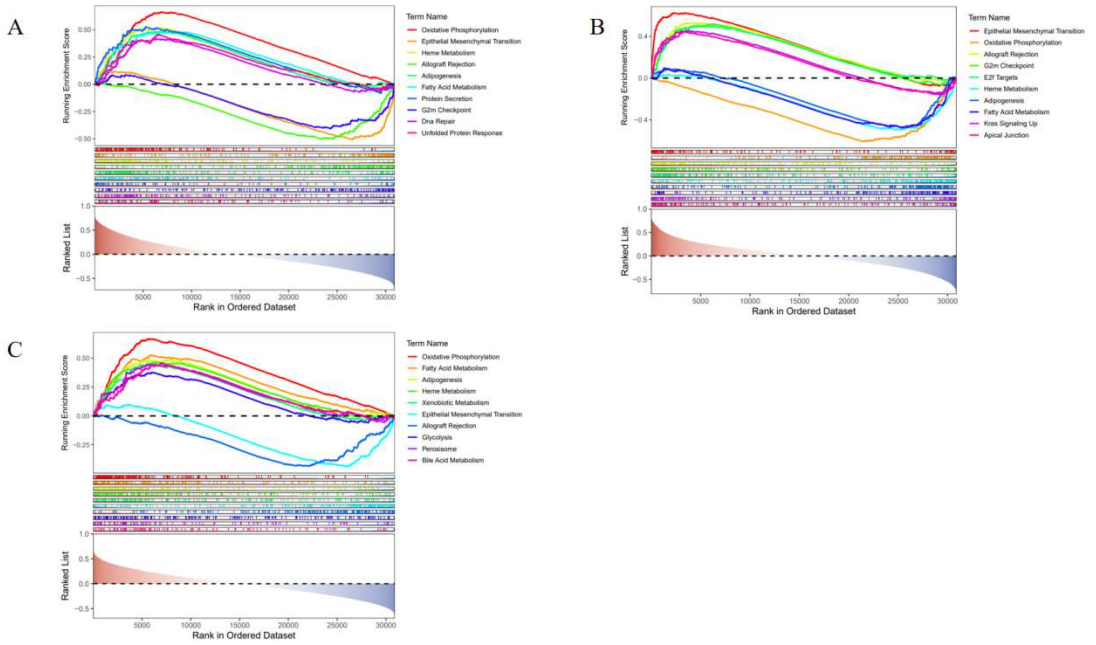

A
Running Enrichment Score
Ranked List
Rank in Ordered Dataset
Term Name
Oxidative Phosphorylation
Epithelial Mesenchymal Transition
Heme Metabolism
Allograft Rejection
Adipogenesis
Fatty Acid Metabolism
Protein Secretion
G2m Checkpoint
Dna Repair
Unfolded Protein Response
B
Running Enrichment Score
Ranked List
Rank in Ordered Dataset
Term Name
Epithelial Mesenchymal Transition
Oxidative Phosphorylation
Allograft Rejection
G2m Checkpoint
E2f Targets
Heme Metabolism
Adipogenesis
Fatty Acid Metabolism
Kras Signaling Up
Apical Junction
C
Running Enrichment Score
Ranked List
Rank in Ordered Dataset
Term Name
Oxidative Phosphorylation
Fatty Acid Metabolism
Adipogenesis
Heme Metabolism
Xenobiotic Metabolism
Epithelial Mesenchymal Transition
Allograft Rejection
Glycolysis
Peroxisome
Bile Acid Metabolism

Figure 5.

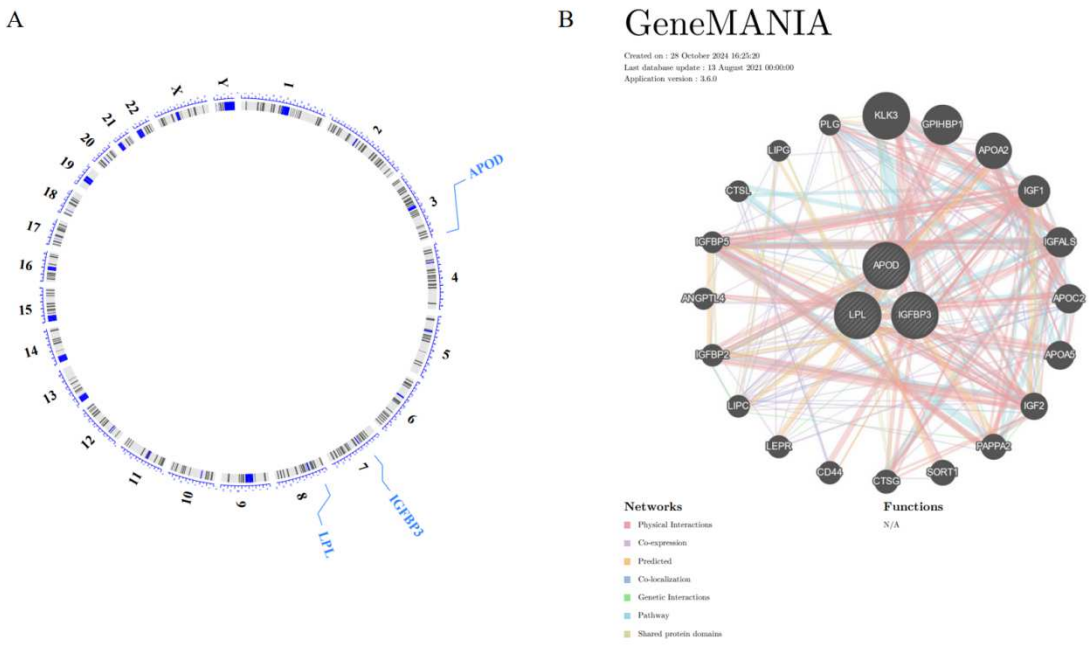

A
APOD
IGFBP3
LPL
B
GeneMANIA
Created on : 28 October 2024 16:25:20
Last database update : 13 August 2021 00:00:00
Application version : 3.6.0
KLK3
PLG
GPIHBP1
LIPG
APOA2
CTSL
IGF1
IGFBP5
IGFALS
APOD
ANGPTL4
LPL
IGFBP3
APOC2
IGFBP2
APOA5
LIPC
IGF2
LEPR
PAPPA2
CD44
CTSG
SORT1
Networks
Physical Interactions
Co-expression
Predicted
Co-localization
Genetic Interactions
Pathway
Shared protein domains
Functions
N/A

Figure 6.

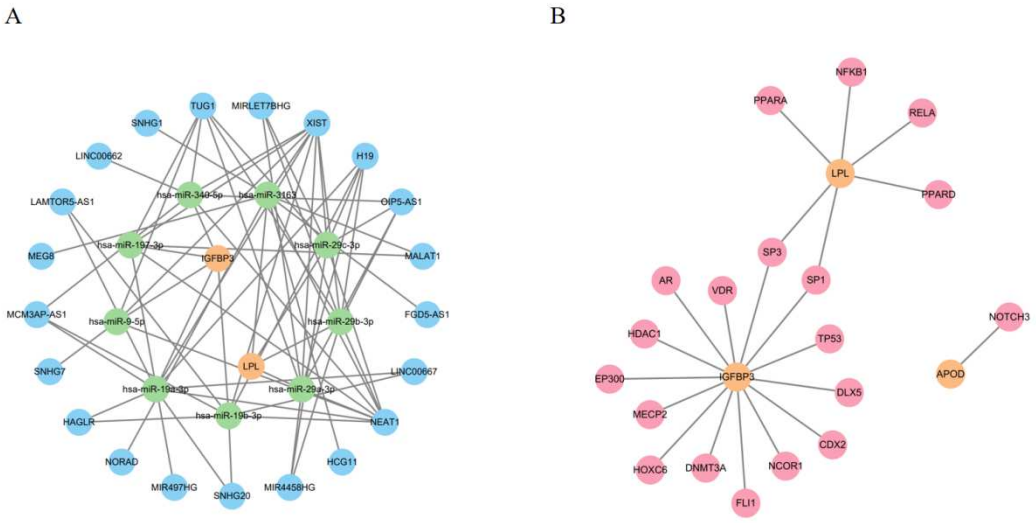

A
TUG1
MIRLET7BHG
SNHG1
XIST
LINC00662
H19
LAMTOR5-AS1
hsa-miR-340-5p
hsa-miR-3163
OIP5-AS1
MEG8
hsa-miR-197-3p
IGFBP3
hsa-miR-29c-3p
MALAT1
MCM3AP-AS1
hsa-miR-9-5p
hsa-miR-29b-3p
FGD5-AS1
SNHG7
LPL
LINC00667
hsa-miR-19a-3p
hsa-miR-29a-3p
HAGLR
hsa-miR-19b-3p
NEAT1
NORAD
HCG11
MIR497HG
SNHG20
MIR4458HG
B
NFKB1
PPARA
RELA
LPL
PPARD
SP3
SP1
AR
VDR
NOTCH3
HDAC1
TP53
EP300
IGFBP3
APOD
DLX5
MECP2
CDX2
HOXC6
DNMT3A
NCOR1
FLI1

Figure 7.

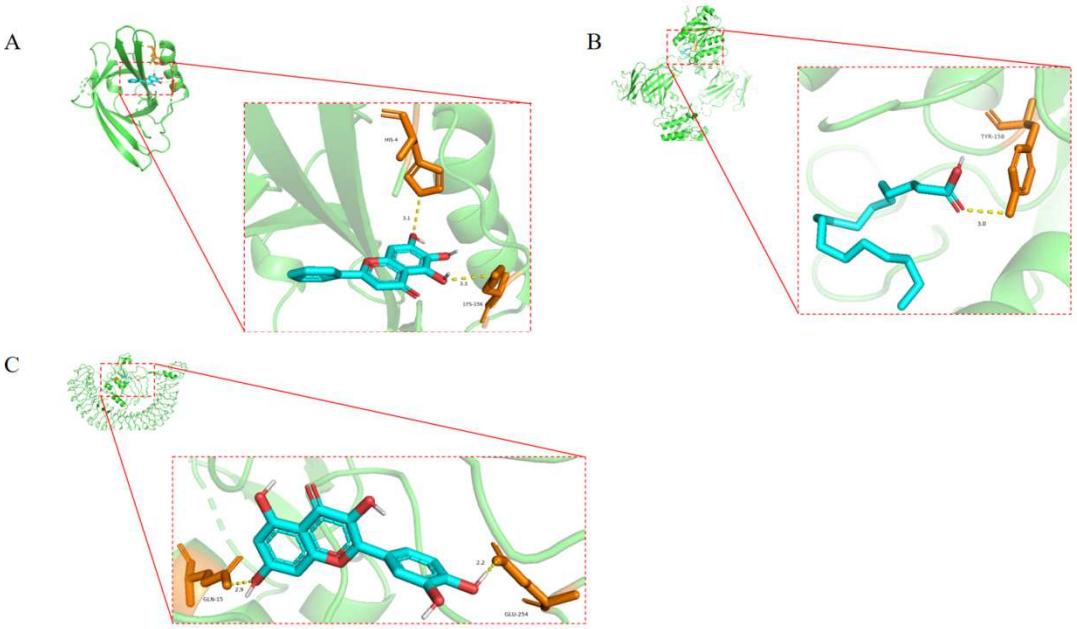


Figure 8.

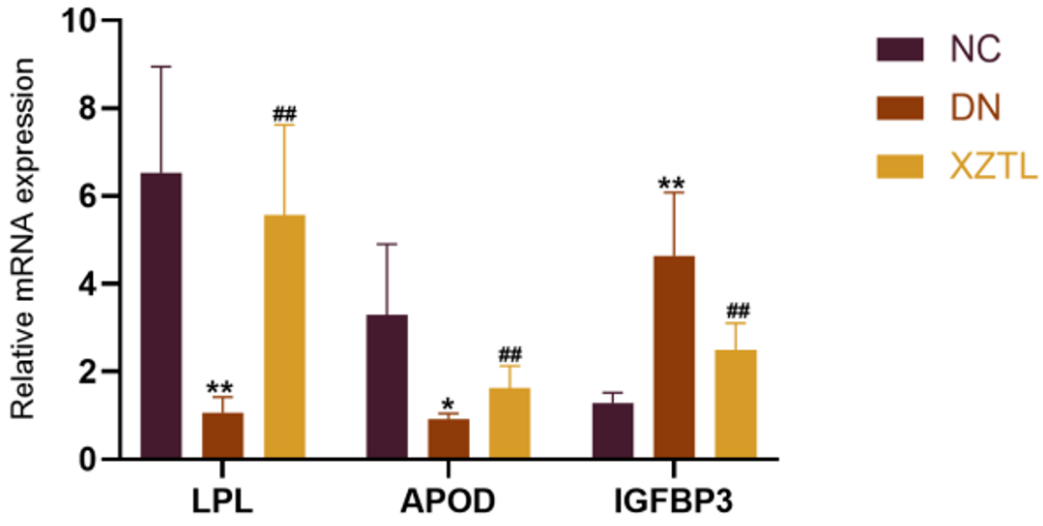

Relative mRNA expression
10
8
6
4
2
0
**
##
*
##
**
##
LPL
APOD
IGFBP3
NC
DN
XZTL

Figure 9.

Supplementary Files

This is a list of supplementary files associated with this preprint. Click to download.

- Table1.xlsx
- Table4.xlsx
- Table3.xlsx
- Table2.xlsx
- Table5.xlsx
- SupplementaryTable11.csv
- SupplementaryTable6.csv
- SupplementaryTable10.csv
- SupplementaryTable7.xlsx
- SupplementaryTable4.csv
- SupplementaryTable9.xlsx
- SupplementaryTable8.xlsx
- SupplementaryTable2.csv
- SupplementaryTable3.csv
- SupplementaryTable5.csv
- SupplementaryTable1.csv